ISSN 1062-8738, Bulletin of the Russian Academy of Sciences. Physics, 2013, Vol. 77, No. 9, pp. 1190–1194. © Allerton Press, Inc., 2013.
Original Russian Text © V.V. Kriventsov, E.P. Yakimchuk, B.N. Novgorodov, D.I. Kochubey, I.L. Simakova, D.A. Zyuzin, D.G. Aksenov, A.V. Chistyakov, A.S. Fedotov, K.V. Golubev, V.Yu. Murzin, M.V. Tsodikov, 2013, published in Izvestiya Rossiiskoi Akademii Nauk. Seriya Fizicheskaya, 2013, Vol. 77, No. 9, pp. 1368–1372.

XAFS Structural Study of Specific Features of the Active Component of Model Palladium Catalysts

V. V. Kriventsov[a], E. P. Yakimchuk[a], B. N. Novgorodov[a], D. I. Kochubey[a], I. L. Simakova[a], D. A. Zyuzin[a], D. G. Aksenov[a], A. V. Chistyakov[b], A. S. Fedotov[b], K. V. Golubev[b], V. Yu. Murzin[b], and M. V. Tsodikov[b]

[a] *Boreskov Institute of Catalysis, Siberian Branch, Russian Academy of Sciences, Novosibirsk, 630090 Russia*
[b] *Topchiev Institute of Petrochemical Synthesis, Russian Academy of Sciences, Moscow, 117912 Russia*
e-mail: kriven@mail.ru

Abstract—Model low-percentage metal oxide palladium catalysts are prepared from acetate complexes of Pd and Mn to study the nature of the activity and the genesis of nanostructured membrane catalyst Pd–Mn systems. A comprehensive study of the prepared model precursor compounds; specific features of their metal components in gels and oxides; and the genesis of the active component, local structure, and charge state is performed by EXAFS and XANES. Possible versions of structural models for the stabilization of metals on oxide supports aare discussed.

DOI: 10.3103/S1062873813090232

INTRODUCTION

A great many studies now focus on developing the targeted formation of heterometallic oxides with high structural organization and porosity. One promising approach to the formation of complex nanostructured metal oxide catalysts is the use of alkoxy [1–3]. Some reports describe results that show the sensitivity of this method to the chemistry of precursors (alkoxides used in conjunction with other metal-complex coreagents, referred to as templates) allow us to perform the targeted formation of structurally organized oxide compounds [4, 5]. The prospect of using this approach to modify the inner surface of porous membrane supports with superfine metal-containing catalytically active coatings was demonstrated in [6, 7]. Membrane catalyst systems based on titanium alkoxide and original heterometallic chelate and acetate complexes of group VI–VIII metals, deposited from stabilized colloidal solutions on the inner surface of the microchannels of ceramic membranes obtained via self-propagating high-temperature synthesis, were prepared in [8, 9]. These systems are effectively used in many important industrial processes. Nanostructured membrane catalyst Pd–Mn systems thus exhibit high catalytic activity in the carbon dioxide reforming of methane to synthesis gas and the conversion of products derived from biomass. It has been found that systems prepared from binary complexes display considerably higher activity than the additive activity of systems synthesized from individual mononuclear complexes.

In this work, model low-percentage metal oxide palladium catalysts were prepared from the acetate complexes of Pd and Mn developed and structurally characterized in [10] to study the nature of the activity and the genesis of nanostructured membrane catalyst Pd–Mn systems. A comprehensive study of the prepared model precursor compounds; specific features of the metal components in their gels and oxides; and the genesis of the active component, local structure, and charge state was performed by EXAFS and XANES.

EXPERIMENTAL

Titanium butoxide and original heterometallic acetate complexes $PdMn(OAc)_4 \cdot H_2O$ with bridging acetate groups of coordination Pd(2+) compounds with Mn(2+) ions were used to synthesize model $PdMn/TiO_2$ oxide systems. The acetate complexes, taken in amounts appropriate for obtaining Pd–Mn/TiO_2 oxide systems containing 2% Pd and 1% Mn, were dissolved in methyl alcohol at $T = 25°C$ and then added to a titanium butoxide solution in toluene under stirring in an Ar stream. Acetate palladium complex $Pd_3(OAc)_6 \cdot CH_2Cl_2$, dissolved in dehydrated benzene at room temperature, was used to prepare a Pd/TiO_2 oxide. A solution containing Pd in amounts appropriate for obtaining a 2% Pd/TiO_2 oxide was then mixed with a titanium *n*-butoxide solution in an Ar stream and stirred with a magnetic stirrer (T = 25°C; 30 min). Next, a stoichiometric amount of water and an aqueous alcoholic solution of $H_2O/C_2H_5OH = 1$ was added dropwise to sols containing precursors of complex metal oxides. After stirring, the solvents were distilled in vacuum (10 mm Hg). The freshly isolated gels were dried and calcined (T = 100°C; 5 h). Oxides were prepared by calcining the gels in an Ar stream ($T = 500°C$; 6 h).

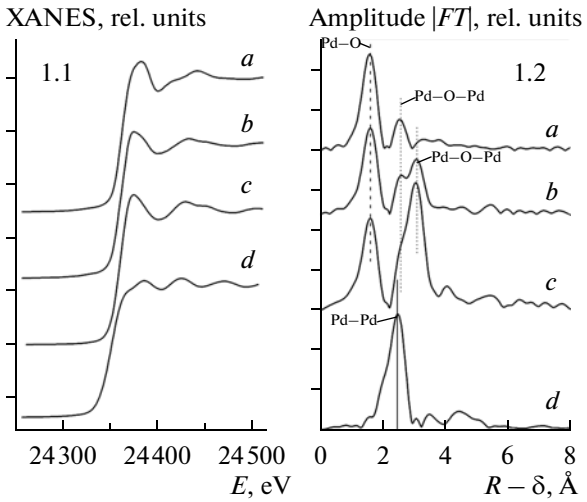

Fig. 1. (1.1) Pd*K*-edge XANES spectra and (1.2) RDF curves of the Pd local environment for the studied samples: (*a*) $PdMn/TiO_2$ gel (sample 1); (*b*) $PdMn/TiO_2$ oxide (sample 2), $T = 500$°C; (*c*) PdO reference compound; and (*d*) Pd^0 foil.

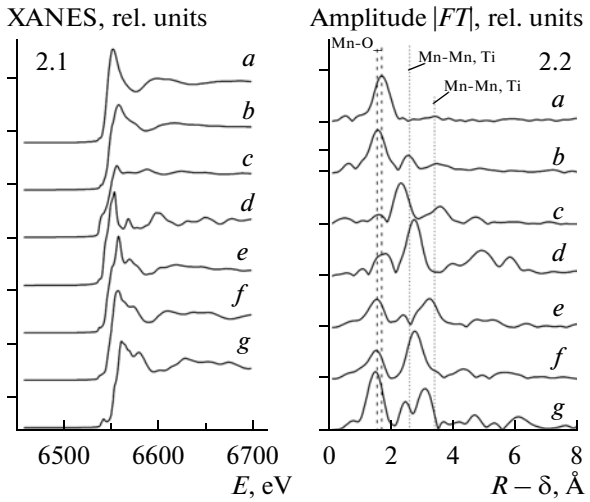

Fig. 2. (2.1) Mn*K*-edge XANES spectra and (1.2) RDF curves of the local Mn environment for the studied samples: (*a*) $PdMn/TiO_2$ gel (sample 1); (*b*) $PdMn/TiO_2$ oxide (sample 2), $T = 500$°C; and reference compounds (*c*) Mn^0, (*d*) MnO, (*e*) Mn_3O_4, (*f*) Mn_2O_3, and (*g*) MnO_2.

X-ray diffraction (XRD) analysis of the samples was carried out using a Philips diffractometer equipped with a graphite monochromator using CuK_α radiation. Elemental analysis was additionally performed for all the samples. According to elemental analysis, almost all of the organic residues were removed during calcination; our $PdMn/TiO_2$ gel (sample 1) and $PdMn/TiO_2$ oxide (sample 2) contained ~2 wt % Pd and ~1 wt % Mn.

EXAFS and XANES spectra (Pd*K*-edge, Mn*K*-edge) of the studied samples were recorded using the EXAFS-spectrometer at the Siberian Synchrotron Radiation Center (Novosibirsk, Russia). The steps for measuring the EXAFS and XANES spectra were 1.5 and 0.3 eV, respectively. X-ray emission was detected using ionization chambers and a fluorescence detector. The oscillating part $\chi(k)$ was isolated using the standard technique in [11, 12]. A Fourier transform value of $k^3\chi(k)$ in the wave number range of 3.0–12.5 $Å^{-1}$ was used to determine the atomic radial distribution function (RDF). Information on the structure (i.e., distances, coordination numbers, and Debye factors) was derived by simulating the spectra (the fitting procedure) with VIPER [12] and EXCURV92 [13] software after preliminary Fourier filtering with the published XRD data for reference bulk compounds at fixed values of the Debye factors ($2\sigma^2 = 0.009$–0.011 $Å^2$).

Preliminary analysis of the particle size distribution was performed by transmission electron microscopy (TEM) using a JEM-2010 microscope. TEM study of the model palladium–manganese catalysts that were precursors of membrane catalyst systems showed that the average sizes of the active component's nanoparticles were approximately the same: ~1.5–2.5 nm.

RESULTS AND DISCUSSION

The Pd*K*-edge XANES spectra and RDF curves (atomic RDFs for the local environment of Pd) for our $PdMn/TiO_2$ gel (sample 1), $PdMn/TiO_2$ oxide (sample 2), and reference palladium compounds are shown in Fig. 1. The Mn*K*-edge XANES spectra and RDF curves (atomic RDFs for the local environment of Mn) for our $PdMn/TiO_2$ gel (sample 1), $PdMn/TiO_2$ oxide (sample 2), and reference manganese compounds are shown in Fig. 2. The structural data (derived from the EXAFS spectra) for the local environment of palladium (*R* is distance, Å; *N* is the coordination number) for samples 1 and 2 and the reference compounds are presented in the table.

It should be noted that it is difficult to use XRD analysis to study this system because the gel samples are completely X-ray amorphous and, in the case of oxides, there is almost no contribution from the considerable diffraction peaks of the active component phases containing Pd and Mn to the total diffraction pattern against the background of the high intensity peaks of the support. XRD analysis allows us to state only that the support (titanium oxide) is crystallized in the anatase structure. Analysis of the Pd*K*-edge XANES spectra for samples 1 and 2 and the reference palladium compounds (Fig. 1.1) suggests that samples 1 and 2 contained only oxide compounds of Pd(2+). No contribution from metallic Pd^0 was detected in the XANES spectra of samples 1 and 2 (within the method's accuracy of 5–10%). It was found for sample 2 that palladium was present mostly in the form of a PdO oxide. The XANES spectrum of sample 2 was in fact similar to that of the reference PdO sample. A detailed comparison of the Pd*K*-edge XANES spectra for samples 1 and 2 (*a*, *b* in Fig. 1.1)

EXAFS data on the local environment of palladium for the studied samples (R is distance, Å; N is the coordination number)

Sample	no. 1 – Pd–Mn/TiO_2 (gel)		no. 2 – Pd–Mn/TiO_2 (oxide)		PdO reference		PdO [14]		Pd^0 [15]	
	R, Å	N	R, Å	N	R, Å	N	R, Å	N	R, Å	N
Pd–O	1.98	4.1	2.00	3.8	2.01	4.0	2.01–2.02	4	–	–
Pd–Pd	2.99	2.0	3.03	2.5	3.02	4.1	3.01–3.03	4	2.74–2.78	12
Pd–Pd	3.50–3.55	~1.0	3.45	3.4	3.43	8.0	3.41–3.44	8	–	–

revealed only slight differences in the shape and features of the spectra; the position of the edge remained unchanged. We may assume that there were contributions from the residues (moieties) of both the Pd–Mn complexes and the PdO nanoparticles.

When compared to the published XRD data for bulk compounds [14, 15], analysis of the EXAFS data (i.e., the RDF curves (atomic RDFs for the local environment of Pd)) and the results from fitting (table) for the investigated samples (Fig. 1.2), suggests the following:

The RDF curves for samples 1 and 2 and the reference PdO compound (*a–c* in Fig. 2) at distances of up to 4.0 Å exhibit several prominent peaks. The first high-amplitude peak (in the region of ~1–2 Å) is attributed to the Pd–O distances; the next peaks were due to the great Pd–Pd distances in the oxide compounds. Samples 1 and 2 contain only oxide compounds of Pd(2+). Metallic Pd^0 was apparently missing from the RDF curves of samples 1 and 2 (within the method's accuracy of 5–10%), since the high-intensity peak of R_{Pd-Pd} = ~2.73–2.78 Å characteristic of the metal (*d*, Fig. 1) was not detected. The final formation of the immediate oxygen environment of Pd (an anion sublattice) for this system occurs at the gel stage (the slight increase in the coordination number (up to 4.1) and the slight shortening of the Pd–O distance (1.98 Å) relative to the reference oxide (~2.01 Å)) can be attributed to the more symmetrical oxygen environment and/or the contribution from the oxygen octahedron of the transition compound resulting from the decomposition of the parent Pd–Mn complex). During the subsequent preparation of the oxide (calcination at T = 500°C), no significant change occurred; the resulting R_{Pd-O} = ~2.00 Å, N = ~3.8 values were close to those of the reference PdO sample, within the method's margin of error.

The formation of a Pd cation sublattice begins during the formation of the gel; the obtained values for the first distance, R_{Pd-Pd} = ~2.99 Å, N = ~2.0, clearly indicate the formation of the palladium oxide nucleation phase. However, it should be noted that after preliminary fitting, the second Pd–Pd distance (~3.50–3.55 Å) has a low coordination number (~1.0) and differs somewhat from the distance for PdO (~3.43 Å).

The Pd cation sublattice finally formed during the preparation of the oxide (calcination at T = 500°C). The obtained R_{Pd-Pd} values of ~3.03 and ~3.45 Å were fairly close to the values for the reference palladium oxide (3.02 and 3.043 Å); however, the respective coordination numbers N of ~2.5 and ~3.4 were lower than for the reference sample (4 and 8, respectively).

These structural data suggest that a highly dispersed PdO nanophase forms and stabilizes on a TiO_2 oxide support. It should be noted that possible distortions of the local structure (compared to the reference PdO sample) for these nanoparticles are apparently due to both size effects and the effect of ions of the second metal, i.e., Mn.

Analysis of the Mn*K*-edge XANES spectra of the investigated samples and the reference manganese compounds (Fig. 2.1) suggests the following:

Samples 1 and 2 contained only oxide compounds of Mn. No contribution from metallic Mn^0 was detected in the XANES spectra of samples 1 and 2. Based on a comparison and detailed analysis of the edge position, shape, and features of the spectra of sample 1 and the reference compounds, we may assume that during the formation of our gel (sample 1), manganese is present mostly in the form of oxide compounds of Mn(2+), while the greatest contribution (at least 70–80%) to sample 2 comes from Mn(3+) compounds. It is also possible that some manganese is present in the form of Mn(4+) compounds, and only a very small portion—no more than 10%—is in the form of Mn(2+) compounds.

Analysis of the EXAFS data (i.e., the RDF curves (atomic RDFs for the local environment of manganese) for the investigated samples and the reference compounds (Fig. 2.2)) as compared to the published XRD data for bulk compounds and the preliminary results from fitting suggests the following:

Samples 1 and 2 contain only oxide compounds of Mn. No contribution from metallic Mn^0 was detected in the XANES spectra of samples 1 and 2. The first high-amplitude peak in the RDF curves for samples 1 and 2 in the region of ~1–2 Å can be attributed to the Mn–O distances. It should be noted that the position of this peak changes upon switching from gel to oxide (the Mn–O distance is shortened appreciably, while the peak amplitude falls slightly). The next two low-

intensity peaks in the RDF curve for sample 2 (in the region of ~2–3 and ~3–4 Å) can be attributed to the Mn–Me (Mn, Ti) distances in the oxide compounds. Peaks like these are not observed for sample 1 (gel): the first peak (in the region of ~2–3 Å) is missing altogether, while the second peak (in the region of ~3–4 Å) has a very low amplitude.

It should be noted that the positions and amplitudes of the Mn–O peaks in the RDF curves (Fig. 2.2) coincide appreciably for sample 2 and the reference Mn_2O_3 and Mn_3O_4 compounds.

On the other hand, this tendency is not observed for the more distant peaks corresponding to the Mn–Mn distances in the RDF curves (Fig. 2.2) for sample 2 and the reference compounds (neither positions nor amplitudes of the peaks coincide with those for the reference samples). The set of distances and coordination numbers derived after preliminary fitting for sample 1 (gel) was $R_{Mn-O} = \sim 2.11$ Å, $N = \sim 4.9$, while the sets for sample 2 (oxide) were $R_{Mn-O} = \sim 2.03$ Å, $N = \sim 4.5$; $R_{Mn-Me\ (Mn,\ Ti)} = \sim 2.96–3.02$ Å, $N = \sim 2$; $R_{Mn-Me\ (Mn,\ Ti)} = \sim 3.7–3.8$ Å, $N = \sim 1$.

Analysis of the literature XRD data for bulk oxide compounds of manganese [16–21] suggests that when the degree of oxidation changes from Mn(2+) to Mn(4+), the average Mn–O distance can vary from ~2.2 to ~1.9 Å. The structure of Mn–Ti–O mixed bulk compounds was thoroughly studied in [22–24], and the average Mn–O distance of the Mn_2TiO_4 compound is ~2.1 Å. Although the structures of some bulk manganese oxide compounds have Mn–Mn distances (~3 Å and about ~3.6–3.9 Å) that are close to the values obtained by fitting for sample 2, the obtained set of distances corresponds best to the structure of TiO_2 anatase [25] ($R_{Ti-O} = \sim 1.94–1.98$ Å, $N = 6$; $R_{Ti-Ti} = \sim 3.0–3.04$ Å, $N = 4$; $R_{Ti-Ti} = \sim 3.74–3.78$ Å, $N = 4$).

It was shown in [26, 27] that Pd–Co systems (synthesized according to similar techniques) produce mixed oxide compounds of complex composition. It is therefore logical to assume the formation of a complex nanophase of MnO_x–TiO_2 interaction. Based on the above, we may assume that upon switching from gel to oxide during calcination at $T = 500$°C, the degree of oxidation changes for a significant portion of the manganese ions. The greatest contribution to sample 1 (gel) apparently comes from oxide compounds of Mn(2+) with a symmetrical immediate oxygen environment (most likely a distorted octahedron). However, the almost complete absence of large distant Mn–Me peaks in the RDF curve suggests that the system is strongly disordered, and it is difficult at present to draw clear conclusions as to the resulting structure of the gel (with respect to manganese).

The greatest contribution (~70–80%) to sample 2 (oxide) comes from oxide compounds of Mn(3+) with a symmetrical immediate oxygen environment (most likely a distorted octahedron). There is some contribution from oxide compounds of Mn(4+) and a negligible contribution from Mn(2+) compounds. We may assume that distorted (defective) MnO_x surface nanophases are also present. To all appearances, however, most of the manganese ions are incorporated into the near-surface structure of the anatase, and could be accompanied by the stabilization of isolated ions localized on defects and the formation of a complex nanophase of the MnO_x–TiO_y interaction.

CONCLUSIONS

A comprehensive study of specific features of the state and genesis of the active component of low-percentage metal oxide catalysts as promising precursors of membrane catalyst systems prepared from acetate complexes of Pd and Mn was performed via EXAFS and XANES. It was found that the formation of a cationic sublattice begins at the gel stage through the formation of a palladium oxide nucleation phase. Palladium in the studied catalysts was in an oxidized state, mostly in the form of a defective PdO nanophase stabilized on a TiO_2 oxide support. The presence of defective surface nanophases MnO_x was revealed. It was determined that a portion of the manganese ions were incorporated into the near-surface structure of the anatase, and this was accompanied by the stabilization of isolated ions localized on defects and the formation of a complex nanophase of MnO_x–TiO_y interaction. It was shown that distortions of the local structure for palladium nanoparticles result from both size effects and the stabilizing effect of ions of the second metal.

ACKNOWLEDGMENTS

This work was performed on equipment at the Center for Collective Use, Siberian Center of Synchronous and Terahertz Radiation, with the support of the Presidium of the Russian Academy of Sciences (program no. 24); the RF Ministry of Education and Science (project no. 14.518.11.7022); the Russian Foundation for Basic Research (project nos. 120301154, 120390840-mol_rf_nr, 120301039, 120390850-mol_rf_nr, 100301005); and the federal target program Scientists and Science Teachers of an Innovative Russia, 2009–2013.

REFERENCES

1. Abe, Y., Gunji, T., Kimata, Y., et al., *J. Non-Cryst. Solids*, 1990, vol. 121, p. 21.
2. Turova, N.Y., Turevskay, E.P., Yanovskaya, M.I., et al., *The Chemistry of Metal Alkoxides*, Kluwer Acad. Publ., 2001.
3. Tanaka, K., Murakami, Y., Imai, T., et al., *Chem. Lett., Chem. Soc. Jpn.*, 2001, p. 1280.
4. Ellert, O.G., Petrunenko, I.A., Tsodikov, M.V., et al, *Sol-Gel Sci. Techol.*, 1997, vol. 8, p. 213.
5. Teleshev, A.T., Vasilyeva, L.N., Nifantyev, E.E., et al., *Russ. Chem. Bull.*, 2003, vol. 52, no. 9, p. 2083.

6. Tsodikov, M.V., Teplyakov, V.V., Magsumov, M.I., et al., *Kin. Catal.*, 2006, vol. 47, no. 1, p. 25.
7. Teplyakov, V.V., Pisarev, G.I., Magsumov, M.I., et al., *Catal. Today*, 2006, vol. 118, p. 7.
8. Teplyakov, V., Tsodikov, M., Moiseev, I., et al., *Proc. Membrane Science and Technology Conf. of Visegrad Countries PERMEA*, Siofok, Sept. 2–6, 2007, p. 39.
9. Loktev, A.C., Parkhomenk, K.V., Dedov, A.G., et al., *Chem. Technol.,* 2008, vol. 5, p. 208.
10. Nefedov, S.E., Vargaftic, M.N., and Moiseev, I.I., *Inorg. Chem. Commun.*, 2006, vol. 5, p. 208; Kozitsyna, N.Yu., Nefedov, S.E., Cherkashina, N.V., et al., *Izv. Ross. Akad. Nauk, Ser. Khim.*, 2005, vol. 9, p. 2149.
11. Kochubei, D.I., *EXAFS-spektroskopiya katalizatorov* (EXAFS Spectroscopy for Catalysts), Novosibirsk: Nauka, 1992.
12. Klementiev, K.V., *J. Phys. D: Appl. Phys.*, 2001, vol. 34, p. 209.
13. Binsted, N., Campbel, J.V., Gurman, S.J., et al., *EXCURV92 Program Code*, SERC Daresbury Lab., 1991.
14. ICSD Collection Code 24692, 26598-Tetragonal PdO.
15. ICSD Collection Code 64915, 64916, 64918 – Pd^0.
16. ICSD Collection Code 42774, 42743 – Mn^0.
17. ICSD Collection Code 28898, 29327 – MnO.
18. ICSD Collection Code 30005 – Mn_3O_4.
19. ICSD Collection Code 24342, 33647 – Mn_2O_3.
20. ICSD Collection Code 16956 – Mn_5O_8.
21. ICSD Collection Code 76430, 20227 – MnO_2.
22. ICSD Collection Code 22313, 28371 – Mn_2TiO_4.
23. ICSD Collection Code 22383, 28325 – $MnTi_2O_4$.
24. ICSD Collection Code 44407, 60006 – $MnTiO_3$.
25. ICSD Collection Code 9852, 9853 – TiO_2 (anatase).
26. Kriventsov, V.V., Novgorodov, B.N., Kochubey, D.I., et al., *Nucl. Instrum. Meth. Phys. Res.: A*, 2007, vol. 575, p. 180.
27. Kriventsov, V.V., Novgorodov, B.N., Yakimchuk, E.P., et al., *J. Surf. Investig. X-Ray, Synchrotron Neutron Techn.*, 2010, vol. 4, no. 4, p. 636.

Translated by M. Timoshinina